Department of Physics and Technology, University of Bergen

Phase Transitions in Non-Equilibrium Dynamical Systems

by

Szabolcs Horvát

Advisor: László P. Csernai
Co-advisor: Jan S. Vaagen

Thesis submitted to University of Bergen in partial fulfillment of the requirements of the Dr. Scient. Degree

October 2010

Contents

Acknowledgements

I am grateful to my supervisor, Prof. László Csernai, for his help during the period of my PhD, useful advices, and especially for always being available for discussions when I needed advice.

I am indebted to my colleagues and collaborators for all the useful and enlightening discussions that we had: Cheng Yun, Sven Zschocke, Etele Molnár, Björn Bäuchle and Zoltán Néda.

I am thankful to my parents for their support during my studies, and especially grateful to Xiao Duo for her support and great encouragement during the past few months.

Bergen, October 2010

Preface

Significance of the subject

Phase transitions are usually described in a quasi-static manner, assuming local phase equilibrium. This approach is not viable when studying rapid and dynamical changes. An area of active research in heavy ion physics is describing the transition from Quark-Gluon Plasma to hadronic matter. This is a rapid transition where non-equilibrium processes play an important role. It is conjectured that the transition proceeds through the Quarkyonic matter phase, where quark deconfinement ceases but freeze-out has not yet occurred. This work presents simple non-equilibrium models for the hadronization that can reproduce experimental observations such as the constituent quark number scaling of the v_2 elliptic flow parameter. The final stages of fluid dynamical expansion, leading up to the hadronization transition, are discussed as well. The study of the final stages of expansion provides guidelines for understanding the transition itself.

Chapter 1

Introduction

1.1 Dynamical phase transitions

Phase transitions are generally described in a quasi-statical way, where it is assumed that local equilibrium persists during the process. However, this is not true for all processes that can be observed in nature. In particular, explosive processes cannot generally be accurately described in such a way, as fluctuations and transport processes, such as heat transfer and viscosity, play an important role.

This work deals primarily with the dynamical phase transitions observed in heavy ion reactions. In ultra-relativistic heavy ion collisions a very hot and dense state of matter is created, where quarks can freely move in a perturbative vacuum, the Quark-Gluon Plasma. This state of matter reaches a thermally equilibrated state, and can be described using relativistic fluid-dynamic models. As the matter expands and cools down, the quarks recombine into observable hadrons, and the fluid-dynamical equilibrium

breaks down. This is a fast and dynamical process that cannot be precisely described using quasi-statical models. It was shown by Csernai and Kapusta that the nucleation rate of the quark deconfinement phase transition is slower than the expansion rate in a heavy ion collision [10, 9]. Therefore chemical equilibrium between the phases and among the hadron species cannot persist during hadronization.

However, such dynamic phase transitions do not only occur under such extreme conditions as those within the collision chamber of a particle collider. These also happen in high temperature detonations used in technical applications, such as rocket engines, gas turbines, internal combustion engines, etc. The correct description of some of these technical applications requires a relativistic treatment despite the slow flow velocities. For example, in a rocket engine, radiation pressure dominates and thus it contributes to stabilizing the detonation front. Thus the results derived from the study of heavy ion reactions may be relevant for several everyday applications.

The Quark-Gluon Plasma is a remarkable state of matter because the quarks and gluons inside it are able to move freely. Thus its study offers an opportunity to better understand the fundamental building blocks of matter. However, this state of matter only exists under extremely high temperatures and energy densities, and cannot be observed directly. As it expands, the quarks are confined into hadrons and the collisions between the hadrons cease (the system "freezes out"). There is evidence supporting that these two processes do not happen exactly at the same time [8]. Between them the matter may exist in the hypothetical Quarkyonic phase [20, 13]. In the experiments only the final hadron spectrum can be measured. To be

able to draw conclusions from these data about the Quark-Gluon Plasma, it is important to understand how the transition to the frozen-out hadronic phase happens.

1.2 Structure of the thesis

This work is a summary of three papers (see references [5, 14, 24]). My main contribution to each one is briefly described below.

1. L. P. Csernai, Y. Cheng, Sz. Horvát, V. Magas, D. Strottman, and M. Zétényi, *Flow analysis with 3-dim ultra-relativistic hydro,* **Journal of Physics G**, vol. **36**, no. 6, p. 064032, 2009.

   My main contribution to the paper is the study of effects of numerical viscosity in computational fluid dynamic calculations and the derivation of analytical expressions suitable for estimating the magnitude of numerical viscosity.

2. Sz. Horvát, V. Magas, D. Strottman, and L. Csernai, *Entropy development in ideal relativistic fluid dynamics with the Bag Model equation of state,* **Physics Letters B**, vol. **692**, no. 4, pp. 277-280, 2010.

   I developed a method to correctly calculate thermodynamic variables during the final stages of expansion in a fluid dynamical model, when the pressure approaches zero, and applied the method to an actual calculation, considering the effects of numerical viscosity. I performed all the necessary analytical and numerical calculations.

3. S. Zschocke, Sz. Horvát, I. Mishustin, L. P. Csernai, *Constituent quark number scaling*, Manuscript

   My contribution to this work is deriving a general formula for calculating the v_2 elliptic flow parameter from a simple source of N moving fireballs, performing the numerical evaluation needed to calculate the evolution of a simple hadronization model, and finally calculating v_2 from the results of the hadronization model. I performed the calculations related to the expansion and recombination phases.

The second chapter describes the results of the first two papers, and deals with interpreting the output of fluid dynamical models during the final stages of expansion in a heavy ion collision. It presents a way to calculate thermodynamic parameters, and the effects of numerical viscosity in computational approaches is discussed.

The third chapter is a summary of the third paper and presents a simple hadronization model that reproduces the constituent quark number scaling of the v_2 elliptic flow parameter.

Results and conclusions are given in each chapter.

1.3 Notations and conventions

In this work we adopt a natural system of units. The speed of light and the Boltzmann constant are considered to be of unit value and dimensionless: $c = 1$ and $k = 1$. In this system of units the value of the reduced Planck constant is $\hbar = \hbar c = 197.326$ MeV fm.

Contravariant components of four-vectors are marked with an upper Greek index:

$$x^\mu = (x^0, x^1, x^2, x^3) = (ct, \mathbf{x}) = (ct, x, y, z)$$

Covariant components have a lower Greek index:

$$x_\mu = (x_0, x_1, x_2, x_3) = (ct, -\mathbf{x}) = (ct, -x, -y, -z)$$

The metric tensor is

$$g^{\mu\nu} = g_{\mu\nu} = \begin{pmatrix} 1 & & & \\ & -1 & & \\ & & -1 & \\ & & & -1 \end{pmatrix}.$$

The Einstein summation convention is used throughout the work, i.e. $a^\mu b_\mu \equiv \sum_{\mu=0,1,2,3} a^\mu b_\mu$.

1.4 Computational fluid dynamics

Fluid dynamics and heavy ion reactions

In the Quark-Gluon Plasma phase, the quarks are thermally equilibrated, thus fluid dynamics suitable for describing this state of matter. Both theoretical considerations [16] and experimental data collected at RHIC suggest that the Quark-Gluon Plasma is an almost perfect fluid with very low viscosity. Csernai et al. have noted that near a critical point of the phase transitions, fluids have a minimal viscosity [11].

Based on these results, the Quark-Gluon plasma can be modelled by a perfect fluid. An ideal relativistic fluid is described by the relativistic Euler equation:

$$\partial_\mu T^{\mu\nu} = 0, \tag{1.1}$$

where $T^{\mu\nu}$ is the energy momentum tensor. For an ideal fluid, $T^{\mu\nu}$ can be expressed as a function of the energy density e and the pressure p using the following formula:

$$T^{\mu\nu} = (e + p)u^\mu u^\nu + pg^{\mu\nu}.$$

Eq. (1.1) expresses the conservation of energy and momentum. When describing nuclear collisions, it is complemented by an equation expressing the conservation of the baryon number:

$$\partial_\mu N^\mu = \partial(nu^\mu) = 0. \tag{1.2}$$

N^μ denotes the four-current of the baryon charge, while n is the invariant baryon-density.

Except for the most trivial configurations, the equations of fluid dynamics can only be solved numerically, on a computer.

The Particle-in-Cell method

There are several computational methods to solve the equations of fluid dynamics numerically.

The numerical fluid dynamical calculations in this work are based on a $(3 + 1)$-dimensional computational fluid dynamics model [6, 2, 5] which uses the Particle-in-Cell method to solve the relativistic Euler-equations. The

Particle-in-Cell method uses a fixed grid of Eulerian cells in conjunction with marker particles that flow through it. The marker particles are Lagrangian fluid cells associated with a fixed amount of baryon charge, and carry momentum and energy between the cells. The marker particles are initially scattered randomly on the computational grid to avoid instabilities. The code runs in a stable way, even up to the very last stages of fluid dynamical expansion.

Chapter 2

Entropy production during the final stages of expansion in heavy ion reactions

2.1 Introduction

In this section we shall deal with the entropy production during the final stages of expansion in ultra-relativistic heavy-ion reactions.

In high energy nuclear collisions a very hot and dense state of matter is created, the quark-gluon plasma. In this state, particles reach thermal equilibrium, thus the most appropriate way of modelling them is relativistic fluid dynamics. As the matter expands and cools, the fluid dynamic equilibrium will be lost, and the quarks will be confined into hadrons. At this point fluid dynamic models cease to be applicable. However, any fluid dynamic calculation will necessarily include the space-time regions where

this happens, and the appropriate interpretation of the results will provide valuable insights about the mechanism of freeze-out and hadronization.

Fluid dynamics alone does not constrain the location of the freeze-out hypersurface. This is determined by external conditions. A viable modelling approach is to let the fluid dynamics simulation run beyond the point of freeze-out and determine the location of the freeze-out hypersurface later from the results, using guidelines such as temperature and density. To be able to do this, we need a reliable way to calculate thermodynamic parameters, such as temperature and entropy, at the final stages of the expansion when the pressure approaches zero. As we will see in the following sections, this problem must be treated carefully.

It must be noted that any *numerical* fluid dynamic calculation will unavoidably contain numerical errors arising from the finite resolution of the computational grid. Some of these numerical errors appear in a form analogous to viscosity. This numerical viscosity will lead to an apparent additional entropy-increase in the computational model, and must not be neglected in a study, especially concerning the entropy and other effects of dissipation.

2.2 Numerical viscosity

Partial differential equations are usually solved numerically on computers by discretising them in some way, and solving the corresponding difference equation. The imprecision resulting from the discretization is called the discretization error. When solving the equations of hydrodynamics numer-

ically, part of the discretization error appears in the form of an additional viscosity.

To see this, let us consider the simple Lax method of solving the one-dimensional continuity equation. The general form of the continuity equation is

$$\frac{\partial \rho}{\partial t} + \nabla \cdot \mathbf{j} = 0,$$

where ρ and j are the density and current of a conserved quantity. $\mathbf{j}$ is usually $\mathbf{j} = \rho \mathbf{v}$, where $\mathbf{v}$ is the flow velocity. The trivial discretisation of this equation in space and time coordinates is

$$\frac{\rho_k^{n+1} - \rho_k^n}{\Delta t} = -\frac{j_{k+1}^n - j_{k-1}^n}{2\Delta x}.$$

(Upper indices represent time, while lower indices represent the space coordinate: $\rho(n\Delta t, k\Delta x) = \rho_k^n$.) However, it turns out that this particular difference equation cannot be used to propagate the solution in time because it leads to instabilities. In the numerical scheme known as the Lax method, the instabilities are removed by replacing the ρ_k^n term on the left-hand side with the average of its spatial neighbours, $\frac{1}{2}(\rho_{k+1}^n + \rho_{k-1}^n)$:

$$\frac{\rho_k^{n+1} - \frac{1}{2}(\rho_{k+1}^n + \rho_{k-1}^n)}{\Delta t} = -\frac{j_{k+1}^n - j_{k-1}^n}{2\Delta x}. \tag{2.1}$$

Let us now expand ρ and j in Taylor series around the point (n, k):

$$\rho_k^{n+i} = \rho_k^n + \frac{\partial \rho}{\partial t} i\Delta t + \frac{\partial^2 \rho}{\partial t^2} \frac{(i\Delta t)^2}{2} + \mathcal{O}(\Delta t^3),$$

$$\rho_{k+i}^n = \rho_k^n + \frac{\partial \rho}{\partial x} i\Delta x + \frac{\partial^2 \rho}{\partial x^2} \frac{(i\Delta x)^2}{2} + \mathcal{O}(\Delta x^3),$$

$$j_{k+i}^n = j_k^n + \frac{\partial j}{\partial x} i\Delta x + \frac{\partial^2 j}{\partial x^2} \frac{(i\Delta x)^2}{2} + \mathcal{O}(\Delta x^3).$$

Substituting the expansions into equation (2.1) we get

$$\frac{\partial \rho}{\partial t} + \frac{\partial^2 \rho}{\partial t^2}\frac{\Delta t}{2} - \frac{\Delta x^2}{2\Delta t}\frac{\partial^2 \rho}{\partial x^2} = -\frac{\partial j}{\partial x} + \mathcal{O}(\Delta x^2, \Delta t^2),$$

and we can see that eq. (2.1) can be interpreted as the discretization of the following continuity equation with a diffusion term:

$$\frac{\partial \rho}{\partial t} + \frac{\partial j}{\partial x} = 0 + \underbrace{\frac{\Delta x^2}{2\Delta t}}_{D}\frac{\partial^2 \rho}{\partial x^2} + \mathcal{O}(\Delta x^2, \Delta t), \tag{2.2}$$

where $D = \frac{\Delta x^2}{2\Delta t}$ is a diffusion coefficient dependent on the parameters of the numerical solution (cell size Δx and time step Δt).

It can be proven that for the difference equation (2.1) to be stable, it is necessary that $|v_k^n|(\Delta t/\Delta x) \leq 1$ for all (n, k) (the Courant condition). This is satisfied if $\varepsilon = \Delta t/\Delta x \leq 1/v_{\max} = \text{const}$. So $D = \frac{1}{2}\varepsilon \Delta x$, and equation (2.2) can be written as

$$\frac{\partial \rho}{\partial t} + \frac{\partial j}{\partial x} = 0 + \frac{\Delta x}{2\varepsilon}\frac{\partial^2 \rho}{\partial x^2} + \mathcal{O}(\Delta x^2, \Delta t). \tag{2.3}$$

Since ε is required to be less than a constant for stability, the diffusion term in this equation decreases linearly (and not quadratically) with Δx.

The equations of fluid dynamics can be written in the form of conservation laws (i.e. continuity equations) for the energy, momentum and particle number (or other conserved charge):

$$\begin{aligned} \frac{\partial e}{\partial t} + \nabla \cdot (\mathbf{v}e) &= -\nabla \cdot (\mathbf{v}P) \\ \frac{\partial M_k}{\partial t} + \nabla \cdot (\mathbf{v}M_k) &= -\frac{\partial P}{\partial x_k}, \qquad k = 1, 2, 3 \\ \frac{\partial n}{\partial t} + \nabla \cdot (\mathbf{v}n) &= 0 \end{aligned}$$

Here e, $\mathbf{M}$ and n are the density of the energy, momentum and particle number. To have a solvable problem, these continuity equations need to be

supplemented by an equation of state connecting these three quantities with the pressure P.

If diffusion terms are added to these three continuity equations, they will correspond to heat transfer, viscosity, and particle diffusion, respectively. Let us look at viscosity in particular.

The usual form of the one-dimensional Euler equation of fluid dynamics, and the continuity equation for the conservation of mass are

$$\rho\left(\frac{\partial v}{\partial t}+v\frac{\partial v}{\partial x}\right)=-\frac{\partial p}{\partial x}$$
$$\frac{\partial \rho}{\partial t}+\frac{\partial(\rho v)}{\partial x}=0.$$

By multiplying the second equation and adding it to the first we obtain the continuity equation for the momentum density, $\mathbf{M}=\rho\mathbf{v}$:

$$\frac{\partial(\rho v)}{\partial t}+\frac{\partial(\rho v^2)}{\partial x}=-\frac{\partial p}{\partial x}.$$

Using the Lax method to approximate the solution of these two continuity equations will in fact give the solution of the following equations containing diffusion terms:

$$\frac{\partial \rho}{\partial t}+\frac{\partial(\rho v)}{\partial x}=0+\frac{\Delta x^2}{2\Delta t}\frac{\partial^2\rho}{\partial x^2}+\mathcal{O}(\Delta x^2,\Delta t)$$
$$\frac{\partial(\rho v)}{\partial t}+\frac{\partial(\rho v^2)}{\partial x}=-\frac{\partial p}{\partial x}+\frac{\Delta x^2}{2\Delta t}\frac{\partial^2(\rho v)}{\partial x^2}+\mathcal{O}(\Delta x^2,\Delta t).$$

If we transform the continuity form of these equations back to the standard form of the Euler equation, we get

$$\rho\left(\frac{\partial v}{\partial t}+v\frac{\partial v}{\partial x}\right)=-\frac{\partial p}{\partial x}+\underbrace{\rho\frac{\Delta x^2}{2\Delta t}}_{\eta_{\text{num}}}\frac{\partial^2 v}{\partial x^2}+2\frac{\Delta x^2}{2\Delta t}\frac{\partial \rho}{\partial x}\frac{\partial v}{\partial x}+\mathcal{O}(\Delta x^2,\Delta t).$$

Comparing this equation with the one-dimensional Navier-Stokes equation, we see that the term $\left(\rho\Delta x^2/(2\Delta t)\right)\left(\partial^2 v/\partial x^2\right)$ is analogous to the viscosity term. Since this term appears as a result of discretisation, its coefficient can be interpreted as the magnitude of the numerical viscosity, η_{num}.

$$\eta_{\text{num}} \sim \rho\frac{\Delta x^2}{2\Delta t}. \tag{2.4}$$

As mentioned earlier, $\Delta x/\Delta t = \varepsilon$ needs to have an upper bound for the numerical method to be stable, therefore the numerical viscosity decreases linearly with the cell size of the grid on which the calculation is done.

Eq. (2.4) allows us to estimate the magnitude of numerical viscosity in computational fluid dynamical calculations.

The numerical viscosity leads to a corresponding increase in entropy even if an adiabatic state in change was assumed in the solved analytic partial differential equations. Fig. 2.1 illustrates this for a calculation describing a $65 + 65$ A·GeV nuclear collision. Note that even the initial entropy depends on the cell size of the computational grid. This is due to the averaging effect of discretisation: the matter is considered to be in equilibrium inside each computational cell. Thus halving the grid-resolution by merging cell-pairs is equivalent to letting each cell-pair reach a thermodynamic equilibrium, which increases the entropy of the system. The lower the resolution of the computational grid, the higher the entropy of the initial state will be.

Numerical viscosity is unavoidable in computational fluid dynamics, therefore it is important the understand the effects and impact of numerical viscosity on the final result. The equations of ideal relativistic fluid dynamics are unstable by nature, and any small perturbation to a stationary solution

will increase [4]. In realistic situations, however, there is always at least a small amount of viscosity and dissipation present, which stabilizes solutions. As seen in the calculations above, it is in fact the introduction of the numerical viscosity that allows the equations of ideal fluid dynamics to be solved in a stable manner on a computer. In a calculation that includes physical viscosity explicitly, it is difficult to estimate the effects and contribution of numerical viscosity. An alternative approach, which we have taken here, is to adjust numerical viscosity so that it becomes approximately equal to the physical viscosity that we wish to describe. The Quark-Gluon Plasma was shown to behave like a low viscosity fluid, so this approach is feasible when describing it. The Particle-in-Cell method that we used runs stably for a wide range of densities from the start of the expansion up to the final stages when the pressure becomes low. The random placement of marker particles helps avoid grid related instabilities and ensures that the results of the calculation will not be strongly affected by the grid size and time step. Therefore this numerical method is suitable for such an approach.

The entropy increase due to numerical viscosity is around 5-6% in our numerical calculations (see figure 2.1). This effect is larger in our $(3+1)$ dimensional model than the one found in $(1+1)$ or $(2+1)$ dimensional calculation [1, 22]. However, it is smaller than the 6-24% increase in models that explicitly include physical viscosity.

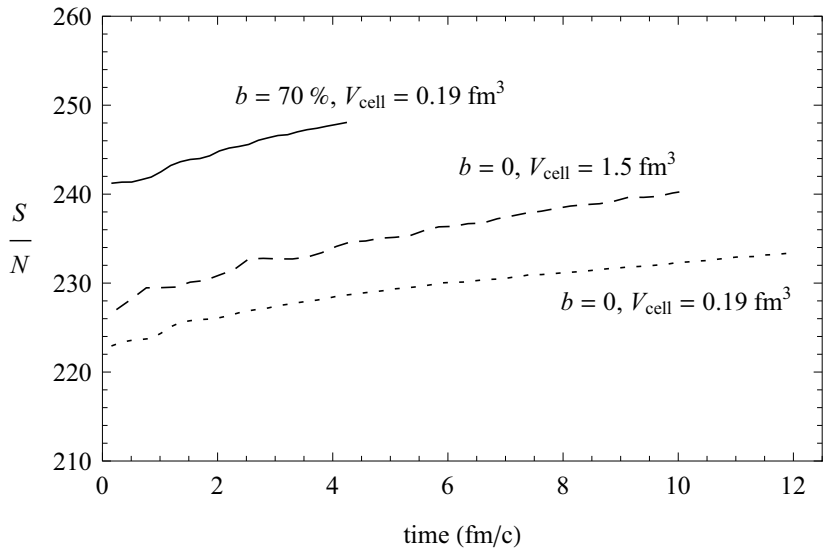

Figure 2.1: Development of the mean specific entropy for three different 3D computational fluid dynamic simulation done using the Particle-in-Cell method. Even though the computation assumed an ideal fluid and adiabatic expansion, the entropy is increasing as a result of numerical viscosity. The entropy increase is about 5-6%. The calculations describe an Au+Au heavy-ion collision at $65 + 65$ A·GeV with impact parameter b. V_{cell} is the size of the computational cells. The difference in the initial specific entropy in the two cases describing a collision with impact parameter $b = 0$ is due to the finite cell size. Due to the averaging effect, the entropy of the same initial state will be larger if it is discretized on a coarser grid.

2.3 The MIT Bag model EoS in fluid dynamics computations

When solving the Euler-equations of fluid-dynamics, it is necessary to complement them with an equation that connects the pressure with the baryon charge and energy density. In our calculations, the simple MIT Bag model equation of state was used to obtain this relationship.

The MIT Bag model of nucleons assumes that the quarks move in perturbative vacuum that has a constant energy density. This energy density, denoted B, is called the Bag constant.

Assuming that the gas of asymptotically free quarks can be modelled using a simple Stefan–Boltzmann gas, and neglecting the baryon charge, the MIT Bag model equations of state are

$$\begin{aligned} E &= \sigma_{\mathrm{SB}} T^4 V + BV \\ p &= \frac{1}{3}\sigma_{\mathrm{SB}} T^4 - B \\ S &= \frac{4}{3}\sigma_{\mathrm{SB}} T^3 V, \end{aligned} \tag{2.5}$$

where σ_{SB} is a constant. The relationship between the pressure and the energy density will be

$$p = \frac{1}{3}e - \frac{4}{3}B \tag{2.6}$$

Note that it is possible to solve the equations of fluid dynamics if only the relationship between the pressure and energy density, eq. (2.6), is given, not the full set of equations of state (2.5). This is applicable to baryonless matter, $n_B = 0$, where the continuity equation is not needed.

It is important to note that the pressure–energy-density relationship of eq. (2.6) allows for negative pressures when the energy density drops below $4B$ (see Fig. 2.2). Negative pressures lead to instabilities in fluid-dynamical computations, therefore we have truncated this $p(e)$ function as follows, for use in numerical fluid dynamics calculations:

$$p = \begin{cases} 0 & \text{if } e < 4B \\ \frac{1}{3}e - \frac{4}{3}B & \text{otherwise} \end{cases} . \tag{2.7}$$

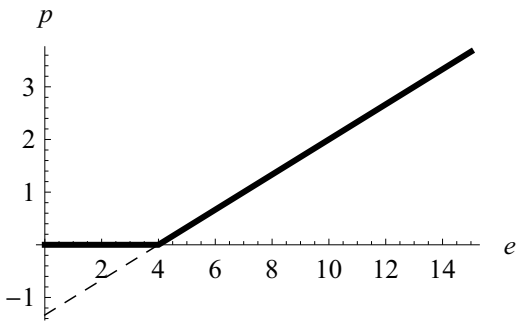

Figure 2.2: The Bag equation of state (pressure–energy-density relationship) used in the fluid dynamical computation. The axes are in units of B.

However, it turns out that there is no single equation of state that is compatible with such a $p(e)$ relationship. Thus the ideal parton gas and the perturbative vacuum in which it moves (referred to as the "Bag field" from now on) cannot be treated as a single thermodynamic system that is in equilibrium. We shall therefore use a simple model where we treat the parton gas and the Bag field as two separate but interacting systems, as illustrated in Fig. 2.3.

To show that eq. (2.7) cannot result from the equation of state of any equilibrated thermodynamical system, let us write the partial derivatives of the entropy $S(T, V)$ with respect to the temperature T and volume V:

$$\left(\frac{\partial S}{\partial V}\right)_T = \frac{1}{T}\left(\frac{\partial E}{\partial V}\right)_T + \frac{p}{T},$$
$$\left(\frac{\partial S}{\partial T}\right)_V = \frac{1}{T}\left(\frac{\partial E}{\partial T}\right)_V.$$

The entropy is a state function, so it must be an exact differential, i.e.

$$\frac{\partial^2 S}{\partial T \partial V} = \frac{\partial^2 S}{\partial V \partial T}.$$

Substituting the partial derivatives into this formula it follows that

$$\left(\frac{\partial E}{\partial V}\right)_T = T\left(\frac{\partial p}{\partial T}\right)_V - p.$$

From this it can be concluded that in the regime of small energy densities, where the pressure is identically zero according to eq. (2.7), the energy does not depend on the volume: $(\partial E/\partial V)_T = 0$.

However, in the regime where $p > 0$, the gas is described by the same equations as the unmodified Bag model, eqs. (2.5), so the energy of the system is proportional to the volume. Thus the $E(T, V)$ internal energy function in these two regimes cannot be stitched together in such a way that a continuous function is obtained.

At the same time, a discontinuity in T does not contradict basic conservation laws as any equation of state with a first order phase transition has a discontinuity on the $[\mu, T]$-plane.

2.4 Interpreting the results of a computational fluid dynamical calculation

A computational fluid dynamic calculation involves the direct calculation of the energy density, pressure, and density of conserved charges, such as the baryon charge in a heavy ion reaction. Thermodynamic quantities such as temperature and entropy do not directly appear in the computation. They can however be calculated from the quantities that we do obtain: energy density and baryon number density.

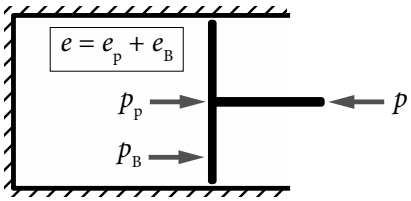

Figure 2.3: Illustration of the compound system consisting of a quark-gas and the Bag field. The effective pressure (that could be measured by an external observer) of the full system is the sum of the pressures of the constituent parts, $p = p_B + p_p$. The Bag pressure, p_B, is always negative: $p_B = -B$ if $e \geq 4B$ and $p_B = -p_p$ if $e < 4B$.

In order to do be able to do this, we need the full equation of state connecting these quantities. In this particular case, however, we have two compound systems, the quark gas and the Bag field. The energy density

obtained from the fluid dynamic computation needs to be decomposed into the energy density of these two parts:

$$e = e_p + e_B$$

(Quantities describing the parton gas will be marked with a p subscript, quantities describing the Bag field will be marked with a B subscript.) Then the temperature $T = T_p$ and entropy density $s = s_p$ of the quark gas can be determined from the Stefan-Boltzmann equation of state. Note that the Bag field is homogeneous, isotropic and uniform, thus it does not contribute to the entropy of the system.

First let us consider the case when $e > 4B$ and the total pressure p is positive. Then the Bag energy density is simply taken to be constant, $e_B = B$, according to the standard MIT Bag model. As the system expands, some of the mechanical work done by the quark gas is used for increasing the total energy of the Bag field, $E_B = e_B V = BV$. This can be interpreted as the Bag field having its own negative valued pressure, $p_B = -B$, while the effective pressure of the compound system is the sum of the pressures of the sub-systems: $p = p_p + p_B = p_p - B$.

$$\begin{aligned} e_p &= \sigma_{\mathrm{SB}} T^4 & e_B &= B \\ p_p &= \frac{1}{3}\sigma_{\mathrm{SB}} T^4 & p_B &= -B \\ s_p &= \frac{4}{3}\sigma_{\mathrm{SB}} T^3 & s_B &= 0 \end{aligned} \tag{2.8}$$

When $e < 4B$, the total pressure of the system is $p = 0$, i.e. the negative Bag pressure must balance the partonic pressure exactly: $p_B = -p_p$. To be able to do decompose the energy density into $e = e_p + e_B$ in this case,

explicit assumptions need to be made about the nature of energy exchange between the two sub-systems. Three choices will be considered here.

- The *first* one is that the energy density of the Bag field is constant during the expansion, $e_B = B$. The mechanical work done by the parton gas component on the Bag field is not enough to maintain a constant Bag energy density. In order for this to be possible, additional energy must be transferred non-mechanically from the gas to the Bag field. As a result of this non-mechanical energy transfer, the entropy of the parton gas component will decrease. Note that even though the fluid dynamic calculation assumed an ideal fluid, and thus the combined parton gas + Bag system can be considered to expand "adiabatically", the expansion of the gas component alone will not be adiabatic, and its entropy will not stay constant the expansion. (This situation is similar to a system with two phases of the same material.)

  A net entropy decrease in an isolated system, such as a quark gas expanding in vacuum, is not physical, as it contradicts the second law of thermodynamics. Thus the assumption that the Bag energy density stays constant is not realistic.

- The *second* case is assuming that the only kind of energy exchange between the sub-systems is a mechanical one. Thus the expansion of the parton gas component is adiabatic, and its total entropy stays constant, $dS = 0$. To see how the energy density of the Bag field will change during the expansion, first let us calculate the energy density of the parton component. Using the equation of state of an ideal

Stefan-Boltzmann gas, eq. (2.8), it can be shown that if the entropy stays constant during the expansion, $S = S_0$, then $e_p/e_{p0} = (V/V_0)^{-4/3}$, where V is the volume of the system. Here the lower index 0 is used to denote quantities at the exact moment when the total pressure of the compound system becomes $p_0 = p_{p0} + p_{B0} = 0$. At this point the energy densities are $e_0 = 4B$, $e_B = B$ (as in the unmodified Bag model), and $e_p = 3B$. Since the total energy $E = E_p + E_B$ is conserved during the expansion, $E_0 = E$ and the volume ratio can be expressed using the energy density ratio: $eV = e_0 V_0 = 4BV_0$ and

$$\frac{e_p}{e_{p0}} = \frac{e_p}{3B} = \left(\frac{V}{V_0}\right)^{-\frac{4}{3}} = \left(\frac{e}{4B}\right)^{\frac{4}{3}} = \left(\frac{e_p + e_B}{4B}\right)^{\frac{4}{3}}.$$

Using the expression of $e_p(T)$ from eq. (2.8), $e_B(T)$ can be calculated as a function of temperature using the following implicit equation:

$$\frac{e_p(T)}{3B} = \left(\frac{e_p(T) + e_B(T)}{4B}\right)^{\frac{4}{3}}. \tag{2.9}$$

- The *third* choice is that the energy of the parton gas in a Lagrangian cell (i.e. a region of space that moves together with the flow) is constant: $dE_p = 0$. This is only possible if in addition to the mechanical work that the quark gas component does on the Bag component, energy is transferred non-mechanically from the Bag to the quark gas, resulting in a zero net energy exchange between the two sub-systems. The entropy of the parton gas will increase during this process. This corresponds to a dissipative expansion.

  If $E_p = \text{const.}$, then $E_B = E - E_p$ is also a constant because the total energy E of the system is conserved. The ratio $E_B/E_p = e_B/e_p$ will

not change during the expansion, thus

$$e_B(T) = \frac{e_p(T)}{3}. \tag{2.10}$$

- If the net energy transfer is directed from the Bag component towards the parton gas, then the entropy increase will be even larger.

The energy density of the Bag field, e_B, is plotted as a function of temperature in Fig. 2.4 for the three assumptions discussed above. In these calculations, the value of the Bag constant was taken to be $B = 396$ MeV/fm^3.

The *interaction measure* was also calculated for these three cases for the purpose of comparison with Lattice QCD simulations. The interaction measure is usually defined as

$$\mathrm{IM} = (\hbar c)^3 \frac{e - 3p}{T^4}. \tag{2.11}$$

Notice that for an ideal Stefan-Boltzmann gas, where the particles do not interact, the value of the interaction measure, is IM = 0. The stronger the interaction between the particles, the more the interaction measure will differ from zero.

When $p > 0$, based on eq. (2.5) the interaction measure decreases with T^{-4}:

$$\mathrm{IM}(T) = (\hbar c)^3 \frac{4B}{T^4}$$

When $p = 0$, then $\mathrm{IM}(T) = (\hbar c)^3(e_p(T) + e_B(T))/T^4$. Different results are obtained depending on the assumption made about the energy transfer between the sub-systems.

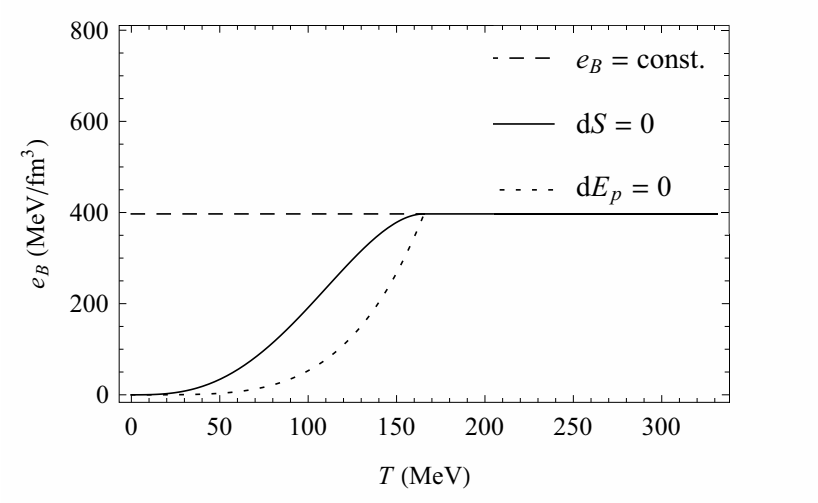

Figure 2.4: The energy density of the Bag field, e_B, as a function of the temperature T. The dashed line represents the case when e_B is constant during the expansion. This has been shown to be unrealistic is it leads to entropy decrease. The solid line corresponds to the constant entropy case, S = const., while the dotted line corresponds to the total energy of the parton gas component staying constant during expansion, E_p = const. In the latter two cases the energy density of the Bag decreases as the system expands.

If $e_B = B$ = const., then

$$\mathrm{IM}(T) = (\hbar c)^3 \left(\sigma_{\mathrm{SB}} + \frac{B}{T^4} \right)$$

If the entropy of the parton gas component stays constant, then using

eq. (2.9) we obtain

$$\mathrm{IM}(T) = (\hbar c)^3 \left(\frac{e_p(T)}{3B}\right)^{\frac{3}{4}} \frac{4B}{T^4} = \\ = (\hbar c)^3 \left(\frac{\sigma_{\mathrm{SB}}}{3B}\right)^{\frac{3}{4}} \frac{4B}{T}.$$

If the total energy of the parton gas stays constant during the expansion, then using eq. (2.10) we get a constant interaction measure.

$$\mathrm{IM}(T) = (\hbar c)^3 \frac{4}{3}\sigma_{\mathrm{SB}}.$$

These three cases are summarized and plotted in Fig. 2.5. If the net energy transfer is directed from the Bag to the parton gas, then the interaction measure curve decreases with expansion when $p = 0$. In the same figure the results of a Lattice QCD calculation [12] are plotted for the purpose of comparison (empty circles). These calculations predict a decrease in the interaction measure as the matter expands. This is possible in our model if more energy is transferred from the Bag field to the gas components, corresponding to a sharper decrease in e_B and a higher entropy increase.

2.5 Applying the method

The method described here was applied to interpret the results of a $(3+1)$-dimensional computational fluid dynamics calculation based on the Particle-in-Cell method, and calculating the entropy as a function of time.

The calculation that was considered describes an Au+Au heavy ion collision at $65 + 65$ A·GeV with impact parameter $b = 0$. The cell size of the computational grid was 0.19 fm^3. The initial state of the calculation

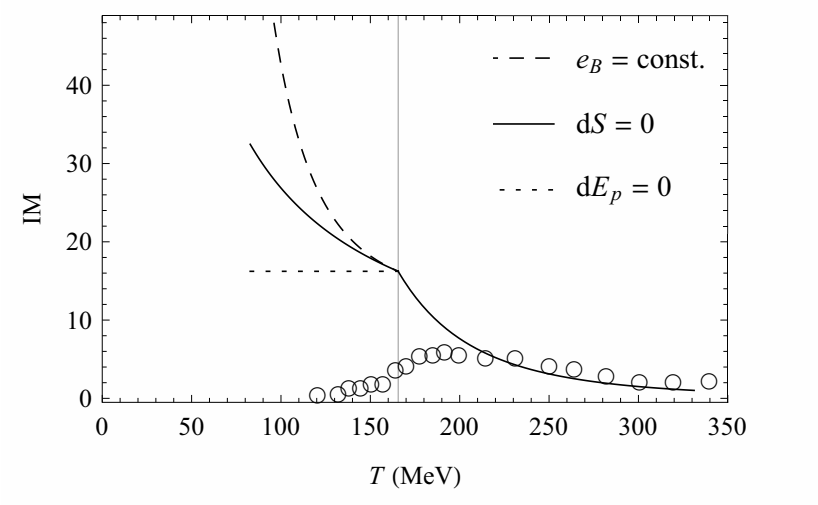

Figure 2.5: The interaction measure, IM, as a function of temperature during expansion. The dashed line corresponds to $e_B = B =$ const. (this case is not physical as itleads to decreasing entropy in the expansion), the solid line corresponds to constant entropy, while the dotted line corresponds to the energy of the parton gas component being conserved during expansion. The result obtained from a Lattice QCD calculation [12] is plotted (empty circles) for the purpose of comparison.

was taken from an analytic string rope model allowing for strings of the colour-magnetic field with differing string tensions [19, 18].

For these calculations a more realistic set of equations of state was used

for the parton gas component [4]:

$$\begin{aligned} e_p &= \frac{1}{(\hbar c)^3}\left(\frac{37}{30}\pi^2 T^4 + \frac{1}{3}\mu_B^2 T^2 + \frac{1}{54\pi^2}\mu_B^4\right) \\ p_p &= \frac{1}{(\hbar c)^3}\left(\frac{37}{90}\pi^2 T^4 + \frac{1}{9}\mu_B^2 T^2 + \frac{1}{162\pi^2}\mu_B^4\right) \\ n_p &= \frac{1}{(\hbar c)^3}\frac{2}{9}\left(\mu_B T^2 + \frac{1}{9\pi^2}\mu_B^3\right) \\ s_p &= \frac{1}{(\hbar c)^3}\left(\frac{74}{45}\pi^2 T^3 + \frac{2}{9}\mu_B^2 T\right) \end{aligned} \tag{2.12}$$

Here n_p is the baryon number density of the parton gas and μ_B is the baryon chemical potential. Note that for this equation of state it is still true that $p_p = e_p/3$.

From the fluid dynamics code, we obtain the energy density e and baryon number density n (as well as the pressure p). After decomposing the energy density as $e = e_p + e_B$, eqs. (2.12) can be used to solve for the temperature T and baryon chemical potential μ_B, and finally calculate the entropy density s_p. Since eqs. (2.12) is a fourth order polynomial system of equations in two unknowns, the most effective way was to solve it numerically.

The mean specific entropy (total entropy divided by total baryon number, S/N) was calculated for the three assumptions discussed in the previous section. The results are plotted in Fig. 2.6. As expected, assuming that the Bag energy density is constant, $e_B = \text{const.}$, leads to an entropy decrease, which is un-physical because it contradicts the second law of thermodynamics. The entropy of a closed system cannot decrease. The assumption that the total energy of the gas component is constant, $dE_p = 0$, leads to an increase in entropy. If the total energy of the gas increased because extra energy is transferred to it from the Bag, then the entropy would increase even more.

The assumption that the quark gas component expands adiabatically would ideally lead to a constant entropy, however, due to the numerical viscosity of the computational method, there is a slight increase (solid line in Fig. 2.6).

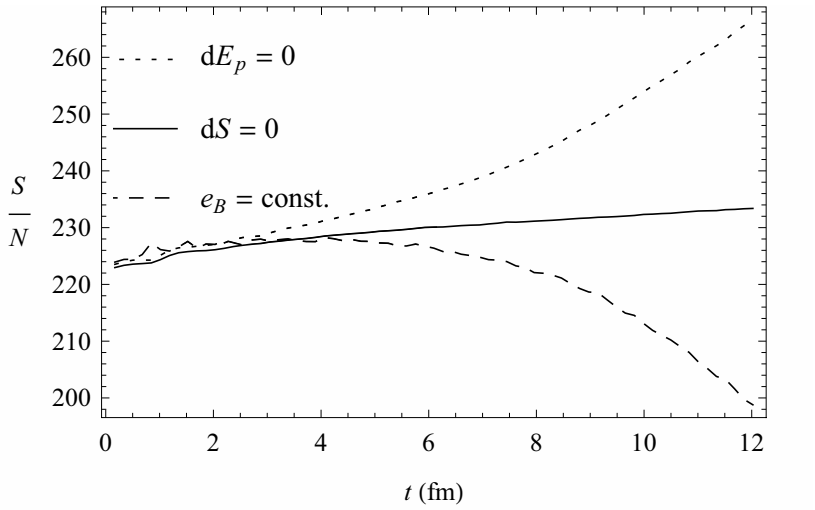

Figure 2.6: Change of the mean specific entropy S/N in time during expansion in a numerical fluid dynamic computation. The dashed line corresponds to the assumption that the Bag energy density is constant. This leads to decreasing entropy, which conflicts with the second law of thermodynamics. The solid line represents an adiabatic expansion of the quark gas component. The slight entropy increase here (of 5-6%) is due to the numerical viscosity of the computational method. The dotted line corresponds to the assumption that the total energy of the gas component is constant during expansion. The cell size was $dx = dy = dz = 0.575$ fm

Chapter 3

Constituent quark number scaling

3.1 Asymmetry of the flow in heavy-ion collisions

The usual way to characterize the asymmetry of the transverse flow of the expanding matter in heavy ion collisions is by using the coefficients of the Fourier expansion of the momentum distribution of particles. Let $f(p_\perp, \varphi, p_z)$ denote the momentum distribution in cylindrical coordinates. $p_\perp$ denotes the transverse momentum, p_z the longitudinal momentum, and φ is the angle in the transverse plane. Then the momentum distribution for mid-rapidity particles can be expanded as

$$f(p_\perp, \varphi, p_z = 0) = n(p_\perp, p_z = 0) \left[1 + \sum_{k=1}^{\infty} v_k(p_\perp) \cos(k\varphi) \right]. \qquad (3.1)$$

The coefficients v_k are used to characterize the asymmetry of the distribution. v_1 corresponds to directed flow, while v_2 corresponds to elliptic flow. A momentum distribution with a non-zero v_2 parameter is shown schematically on figure 3.1.

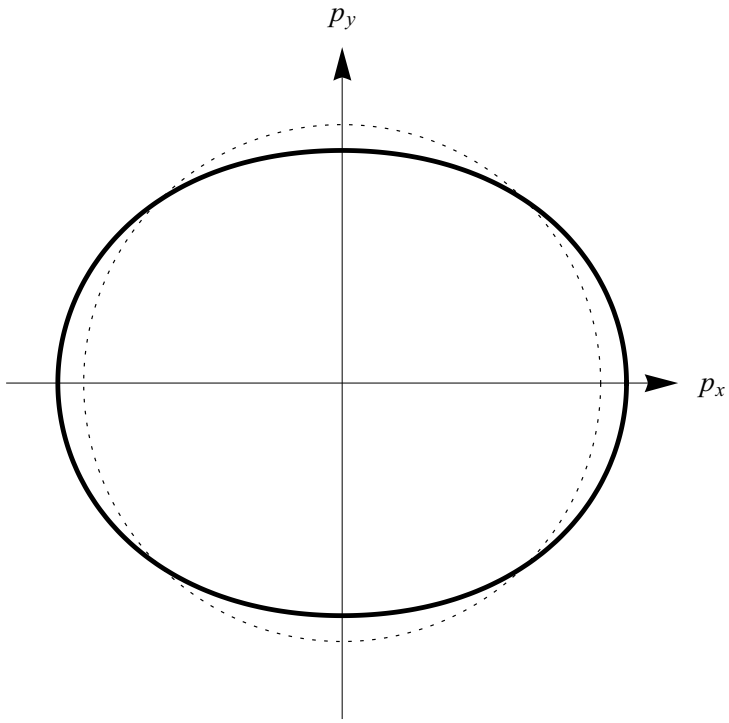

Figure 3.1: Illustration of a momentum distribution with $v_2 \neq 0$ and $v_k = 0$ for $k \neq 2$. A fully symmetric distribution is shown for comparison (thin dashed line).

3.2 Constituent quark number scaling of v_2

It was found in heavy ion collision experiments that the momentum distribution of the detected particles is azimuthally asymmetric in the plane perpendicular to the beam direction. This phenomenon is referred to as the elliptic flow in the literature. The asymmetry is caused by several factors, the main one being the spatially asymmetric state created right after the nuclei collide, due to the non-zero impact parameter.

The v_2 parameter characterizing the elliptic flow is usually studied for mid-rapidity particles, as a function of the transverse momentum, $p_\perp$ (i.e. the component of the particle momentum perpendicular to the beam direction). Observations show that if $v_2(p_\perp)$ is re-scaled by the constituent quark number of the considered hadron type, and v_2/n_{cq} is plotted as a function of $p_\perp/n_{\mathrm{cq}}$, then the obtained curves will coincide for all hadron species, both mesons and baryons. Furthermore, it was found that the scaling is even more precise if instead of the transverse momentum, $p_\perp$, the transverse energy, $E_\perp = \sqrt{m^2 + p_\perp^2} - m$, where m is the particle mass, is used as the dependent variable [17, 23]. A plot of the experimentally measured v_2 is shown in figure 3.2.

This finding suggests that the elliptic flow develops in the Quark-Gluon Plasma phase, before the quarks are recombined into hadrons. Therefore the study of constituent quark number scaling, and the understanding of the phenomenon may provide insight into the Quark-Gluon Plasma phase of matter.

The constituent quark number scaling of the v_2 parameter is a remarkably

simple empirical observation. It is reasonable to expect that it can be explained by a relatively simple theoretical model. We developed a very simple model of hadronization and calculated the resulting v_2 curves.

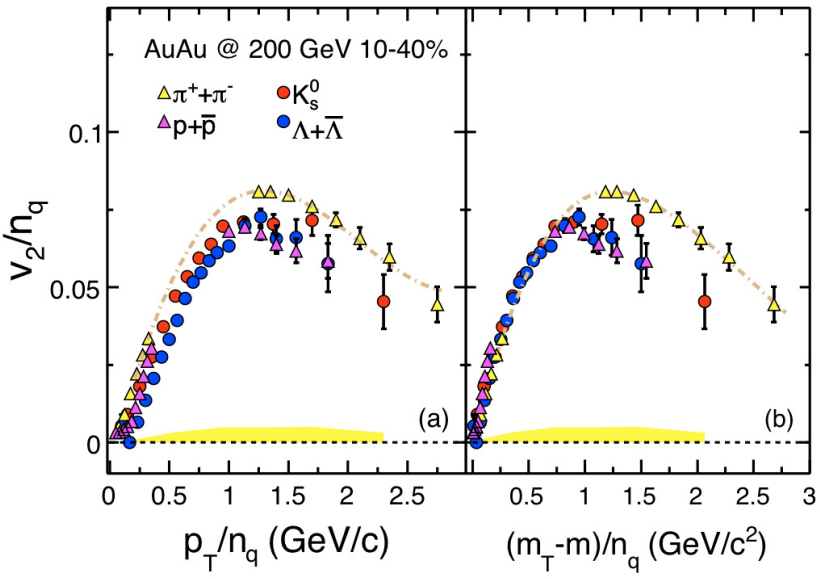

Figure 3.2: Constituent quark number scaling of the v_2 parameter for different hadron species in experimental data [23]. The scaling law is followed more precisely when v_2 is plotted as a function of the transverse mass $m_\perp - m$ (right panel) instead of the transverse momentum (left panel). $m_\perp = \sqrt{m^2 + p_\perp^2}$.

3.3 v_2 scaling in a variable-mass model

Stages of hadronization

We considered a simple model of hadronization where the hadronization happens in several stages during the expansion of a quark gas, as follows:

- The chemical equilibrium between the quarks and anti-quarks and the chiral symmetry breaking starts at the same time.

- As the gas of quarks expands in a background field, the quarks gain mass and become heavier.

- The quarks recombine into hadrons at the same time when the flow freezes out and local thermal equilibrium breaks. This happens at the point where the mean energy per hadron reaches a fixed value (in our model 1.2 GeV, which precedes the empirically observed final freeze-out hadron energy).

The v_2 elliptic flow parameter was calculated at the point of freeze-out. Each of these stages will be described in more detail in the following subsections.

Quark mass in vacuum

The effective mass M of quarks can be calculated based on an effective field theoretical model, the Nambu–Jona–Lasinio model, as a function of

baryon-number density and temperature. The result from [24] is used here:

$$M\left(n_B, T\right) = m - 2\, G_s \langle \overline{q} q \rangle_0 \left(1 - \frac{3\ \sigma_q}{f_\pi^2\ m_\pi^2}\ n_B - \frac{T^2}{8\ f_\pi^2} - \frac{T^4}{384\ f_\pi^4} - \frac{T^6}{288\ f_\pi^6}\ \ln \frac{\Lambda_q}{T}\right) . \tag{3.2}$$

Here m denotes the current quark mass in QGP, T is the temperature and n_B the baryon number density. The values of the constants were taken to be $\langle \overline{q} q \rangle_0 = (0.225\ \text{GeV})^3$, $G_S = 15\ \text{GeV}^{-2}$, $\sigma_q = 15$ MeV, $f_\pi = 93$ MeV, $m_\pi = 138$ MeV, and $\Lambda_q = 300$ MeV [24].

This formula allows interpolating between the current quark mass of the asymptotically free quarks of the QGP and the effective mass of the constituent quarks when chiral symmetry is broken. The dependence of mass on temperature and density is shown in figure 3.3.

Initial state

The initial state of the expansion was chosen from the curve where the quark mass becomes equal to the current quark mass in the baryon density–temperature plane, $[n_B, T]$. The initial state curve is shown in figure 3.4. We assume that at this point the quarks start gaining mass (according to formula (3.2)) and the equilibrium between the chemical potential of quarks and anti-quarks breaks at the same time. Since chemical equilibrium is broken, all calculations need to be done in the density–temperature plane, rather than the baryonic chemical potential–temperature plane ($[\mu_B, T]$). During further expansion, the chemical potentials of quarks and anti-quarks, μ_q and $\mu_{\bar{q}}$, will not be tied to the baryon charge chemical potential, μ_B, and will evolve separately.

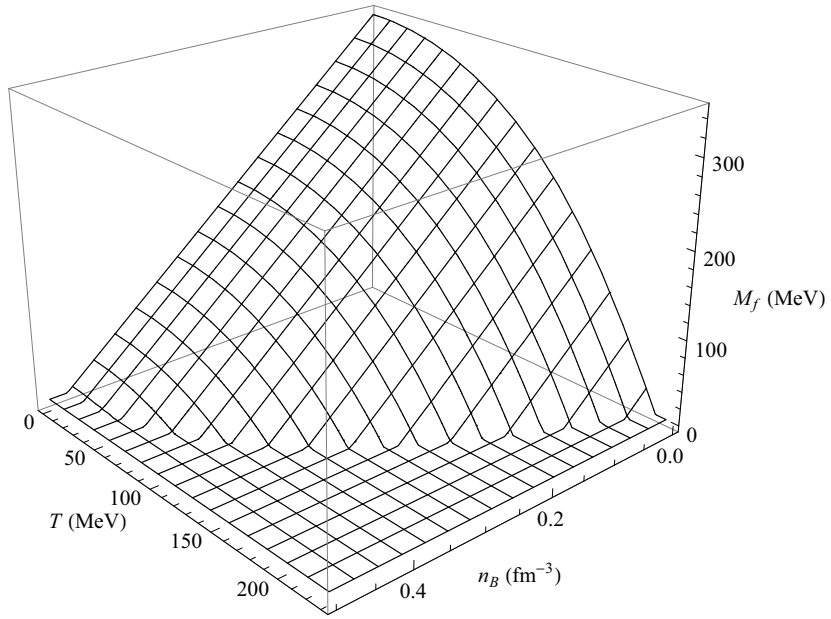

Figure 3.3: Temperature and density dependence of the constituent quark mass, based on eq. (3.2).

The current quark mass is considered to be $m = 7$ MeV, and the mass difference between u and d quarks is ignored.

For simplicity, the quark gas was considered to have Jüttner distribution. To calculate the expansion trajectory of the quark gas, it is necessary to derive the expressions for the energy density (e), particle density (n), and entropy density (s) of a Jüttner gas. This is done in the next section.

Equations of state of the Jüttner gas

The Jüttner distribution is commonly used to describe the distribution of momenta in thermalised relativistic particle systems. Here the particle

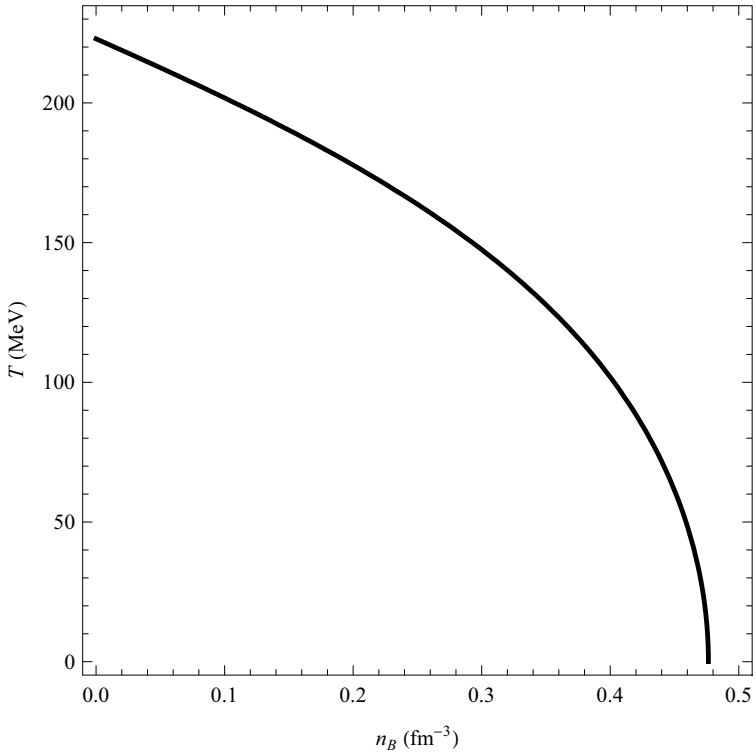

Figure 3.4: The initial state of the expansion was chosen from the curve where the quark mass (shown in figure 3.3) becomes equal with the current quark mass on the $[n_B, T]$ plane.

density, energy density, pressure and entropy density will be derived as a function of temperature, chemical potential and particle mass, assuming a system that follows the Jüttner distribution.

Let us consider a relativistic gas that follows the Jüttner distribution, and calculate the relevant extensive thermodynamic properties as a function of the temperature, T, and chemical potential, μ. The Jüttner distribution

is

$$f(x,p) = \frac{1}{(2\pi\hbar)^3} \exp\left(\frac{\mu - p^\mu u_\mu}{T}\right) \tag{3.3}$$

The invariant particle density can be obtained as

$$n = N^\mu u_\mu = \int p^\mu u_\mu f(x,p) \frac{d^3p}{p^0} \tag{3.4}$$

Substituting (3.3) for $f(x,p)$ we get

$$n = C \int \frac{d^3p}{p^0}\, p^\mu u_\mu\, e^{-p^\mu u_\mu/T},$$

where $C = \frac{1}{(2\pi\hbar)^3} e^{\frac{\mu}{T}}$. The dot product $p^\mu u_\mu$ can be expressed as function of $\mathbf{p}$ as $p^\mu u_\mu = p^0 = \sqrt{\mathbf{p}^2 + m^2}$, where m is the particle mass. Noticing that the integrand is spherically symmetric, it can be written as

$$n = 4\pi C \int_0^\infty p^2\, dp\, e^{-\sqrt{p^2+m^2}/T}.$$

Using the variable transformation

$$\tau = \frac{\sqrt{p^2+m^2}}{T}, \qquad z = \frac{m}{T} \tag{3.5}$$

we obtain

$$n = 4\pi T^3 C \int_z^\infty d\tau\, \tau\sqrt{\tau^2 - z^2} e^{-\tau}.$$

Comparing this result with the integral representation of the modified Bessel function of the second kind,

$$K_n(z) = \frac{2^{n-1}(n-1)!}{(2n-2)!} z^{-n} \int_z^\infty d\tau\, \tau(\tau^2 - z^2)^{n-3/2} e^{-\tau}, \tag{3.6}$$

we find that

$$n = 4\pi C m^2 T K_2(z) = 4\pi C m^2 T K_2(m/T)$$

Using the expression of the energy-momentum tensor in the local rest frame,

$$T^{\mu\nu} = \begin{pmatrix} e & & & \\ & P & & \\ & & P & \\ & & & P \end{pmatrix},$$

and that

$$T^{\mu\nu} = \int \frac{d^p}{p^0}\, p^\mu p^\nu\, f(x,p),$$

we find that the pressure of a Jüttner gas is

$$P = -\frac{1}{3} C \int \frac{d^p}{p^0}\, \left(p^\mu p_\mu - (p^\mu u_\mu)^2\right)\, e^{-p^\mu u_\mu / T}.$$

Performing the same variable transformation as before, eq. (3.5), and comparing the result with eq. (3.6) we get that

$$P = 4\pi C m^2 T^2 K_2(m/T) = nT$$

Analogously, the for the energy density we get

$$e = T^{\mu\nu} u_\mu u_\nu = \int \frac{d^2 p}{p^0}\, (p^\mu u_\mu)^2\, f(x,p),$$

and

$$\begin{aligned} e &= 4\pi C m^4 \left[3\frac{K_2(z)}{z^2} + \frac{K_1(z)}{z}\right] = \\ &= 4\pi C m^4 \left[\frac{3}{4}\frac{K_3(z)}{z} + \frac{1}{4}\frac{K_1(z)}{z}\right], \end{aligned}$$

where $z = m/T$.

The entropy density can be calculated starting from the thermodynamic relation $s = -\mu/Tn + e/T + n$:

$$s = 4\pi C \left(m^3 K_1(z) + m^2 T K_2(z) \left(4 - \frac{\mu}{T}\right)\right).$$

Collecting all results together, the equations of state obtained from the Jüttner distribution are

$$\begin{aligned} n &= 4\pi C m^2 T K_2(z) \\ P &= nT \\ e &= 4\pi C m^4 \left[3\frac{K_2(z)}{z^2} + \frac{K_1(z)}{z} \right] \\ s &= 4\pi C \left(m^3 K_1(z) + m^2 T K_2(z) \left(4 - \frac{\mu}{T} \right) \right), \end{aligned} \tag{3.7}$$

where $z = \dfrac{m}{T}$ and $C = \dfrac{1}{(2\pi\hbar)^3} e^{\frac{\mu}{T}}$

Expansion of the gas

We assume that at the initial moment, chemical equilibrium between quarks and anti-quarks still exists. The based on equation (3.7), the densities of quarks and anti-quarks are

$$\begin{aligned} n_q &= \frac{4\pi}{(2\pi\hbar)^3} e^{\frac{\mu_q}{T}} M(n_B, T)^2 T \, K_2 \left(\frac{M(n_B, T)}{T} \right) \\ n_{\bar{q}} &= \frac{4\pi}{(2\pi\hbar)^3} e^{\frac{\mu_{\bar{q}}}{T}} M(n_B, T)^2 T \, K_2 \left(\frac{M(n_B, T)}{T} \right) \end{aligned} \tag{3.8}$$

In chemical equilibrium, $\mu_q = -\mu_{\bar{q}} = \mu_B/3$ and

$$n_B = \frac{1}{3\pi^2} T \sinh \left(\frac{\mu_B}{3T} \right) M(n_B, T)^2 \, K_2 \left(\frac{M(n_B, T)}{T} \right) \tag{3.9}$$

The initial chemical potentials and quark and anti-quark densities are calculated using these equations. Then the chemical equilibrium breaks and the quark and anti-quarks numbers will be conserved and the densities will change inversely proportionally to the volume V of the system: $n_q = V_0/V n_{q0}$, $n_{\bar{q}} = V_0/V n_{\bar{0}}$, $n_B = V_0/V n_{B0}$, where quantities marked by the

subscript 0 correspond to the initial state of the system. The quark and anti-quark chemical potentials evolve separately and can be obtained from the densities.

We assume that the gas expands adiabatically, i.e. its entropy stays constant during expansion. Using equation (3.7) and the condition that the quark numbers, as well as the baryon charge, are conserved, the quark and anti-quark entropies can be expressed as a function of the baryon charge

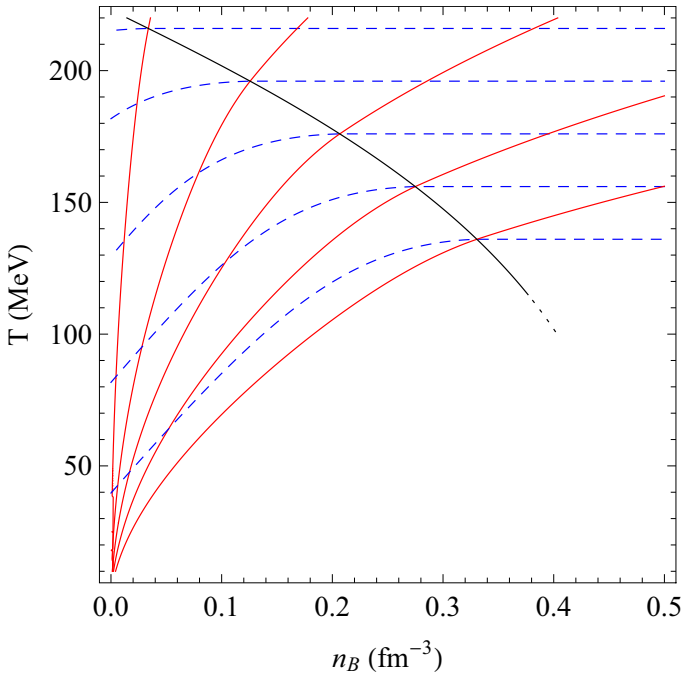

Figure 3.5: The thin red solid lines represent the trajectories of adiabatic expansion, while the thin blue dashed lines represent the trajectories of iso-ergic, dissipative expansion. The thick black line is the initial state curve where quarks masses become equal to the current quark mass.

density n_B and the temperature T (using the initial quark and anti-quark densities). From the condition that the total entropy is conserved,

$$s_0 V_0 = s(n_B, T)\, V = \big(s_q(n_B, T) + s_{\bar{q}}(n_B, T)\big)\, V,$$

the expansion trajectory on the $[n_B, T]$ plane can be calculated. A few possible trajectories, corresponding to different initial conditions, are shown in figure 3.5. The trajectories corresponding to constant energy expansion were also computed and are shown in the same figure. This corresponds to dissipative expansion. Note that the adiabatic expansion leads to the fastest cooling of the gas.

Final state of the expansion

Experimental observations show that the freeze-out happens when the mean energy per hadron reaches approximately 1.0-1.1 GeV [3]. We assume in our model that at this point the quarks recombine into hadrons and local thermal equilibrium ceases to exist between the particles.

The freeze-out line from [3] is represented on the $[\mu_B, T]$ plane in figure 3.6A. The dashed lines are from [3], while the solid lines are computed from the condition that $E_{\mathrm{hadron}}/N_{\mathrm{hadron}} = 1.0$ GeV (1.1 GeV), assuming that the hadrons have Jüttner distribution. The results obtained from the Jüttner gas approximation agree to a $\sim 5\%$ accuracy with the results of the more complete treatment.

In our non-equilibrium model we cannot use the baryonic chemical potential directly, therefore the freeze-out line needs to be approximated

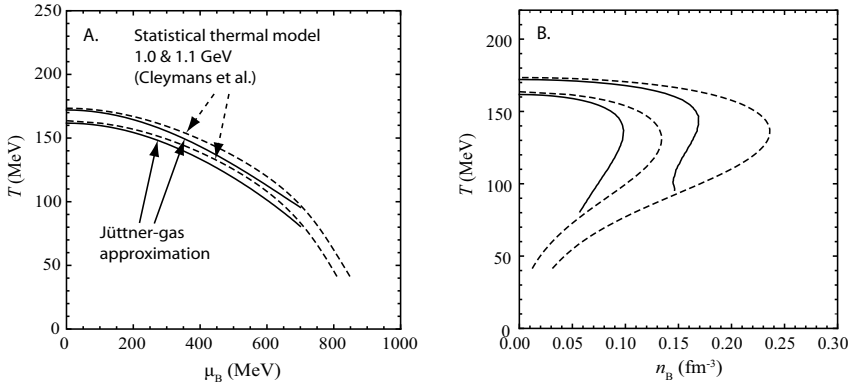

Figure 3.6: Panel A. shows the freeze-out curves on the $[\mu_B, T]$-plane, corresponding to mean energies of $E_{\text{hadron}}/N_{\text{hadron}} = 1.0$ and 1.1 GeV per hadron. The dashed lines are from [3] while the continuous lines were computed assuming that the hadrons have a Jüttner distribution. Panel B. shows the same curves transformed to the $[n_B, T]$ plane.

on the $[n_B, T]$ plane. This is done assuming that hadrons have Jüttner distribution. The results are shown in figure 3.6B.

In our model we assume that at the point of recombination, the hadrons have an average energy of 1.2 GeV / hadron. This energy includes the background field, which is assumed to have an initial energy density of $B = 200$ MeV. To find the freeze-out points, the hadron density must be estimated from the quark and anti-quark densities. This is detailed in the next section. The freeze-out points are shown for some expansion trajectories in figure 3.7.

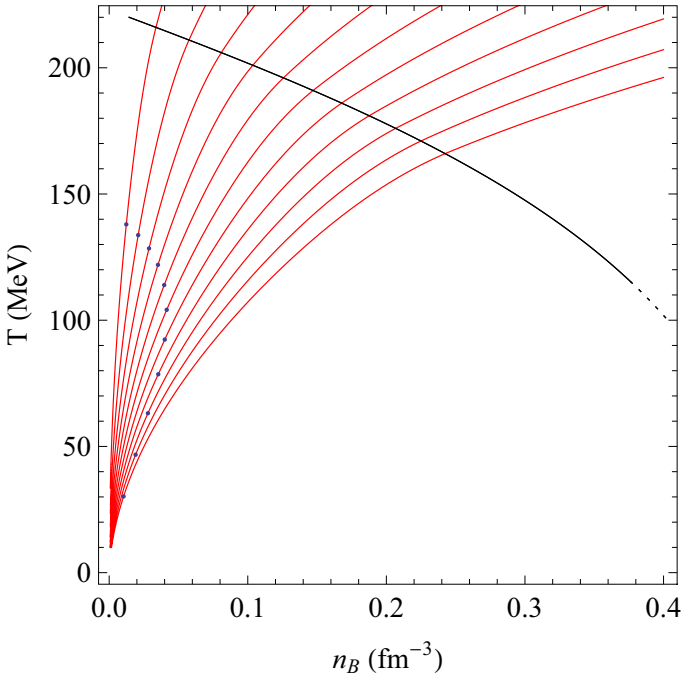

Figure 3.7: The points of freeze-out and hadronization on the expansion trajectories. The points were found based on the condition that the energy of the quarks, including the background field, divided by the estimated number of hadrons that the quarks can recombine into, is 1.2 GeV.

Recombination into hadrons

In this model we assume that the quarks can recombine into three types of hadrons: baryons made of three quarks, anti-baryons made of three anti-quarks, and mesons made of quark–anti-quark pairs.

According to [21], the quark recombination rates are given by

$$q + \bar{q} \to m \quad : \quad \dot{n}_m = C_m \frac{q_m}{g_q g_{\bar{q}}} n_q n_{\bar{q}} \tag{3.10}$$

$$q + q + q \to b \quad : \quad \dot{n}_b = C_b \frac{q_b}{g_q g_q g_q} n_q n_q n_q \tag{3.11}$$

$$\bar{q} + \bar{q} + \bar{q} \to \bar{b} \quad : \quad \dot{n}_{\bar{b}} = C_b \frac{q_b}{g_q g_q g_q} n_{\bar{q}} n_{\bar{q}} n_{\bar{q}}, \tag{3.12}$$

Here n_b, $n_{\bar{b}}$ and n_m denote the baryon, anti-baryon and meson densities, respectively. The dot denotes a time derivative. The an estimate can be given for the hadron densities without fully integrating the rate equations, as follows:

The conserved baryon charge density is

$$n_B = n_b - n_{\bar{b}}.$$

Let a denote the fraction of anti-quarks that recombine into anti-baryons. Then the baryon and anti-baryon densities are

$$n_b = (n_q - n_{\bar{q}})/3 + a n_{\bar{q}}/3, \qquad n_{\bar{b}} = a n_{\bar{q}}/3, \tag{3.13}$$

while the meson density is

$$n_m = (1 - a) n_{\bar{q}}. \tag{3.14}$$

From equations (3.12), the ratio of formed baryons and anti-baryons is $n_b/n_{\bar{b}} = (n_q/n_{\bar{q}})^3 \equiv Q$. From the condition that the quark and anti-quark numbers are unchanged during the recombination process we get

$$a \approx (Q - 1)/(Q^3 - 1). \tag{3.15}$$

Using the parameter a, the baryon and meson densities can be calculated.

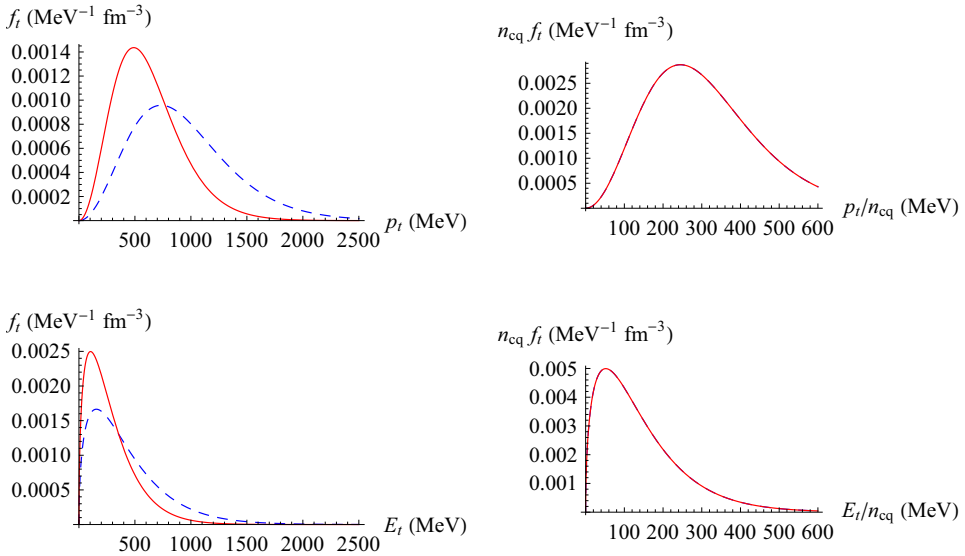

Figure 3.8: Distribution of baryons (blue, dashed) and mesons (red, solid) according to transverse momentum, $p_\perp$, and transverse energy, $E_\perp = \sqrt{M^2 + p_\perp^2} - M$. The right hand panels show the same distributions, re-scaled by the constituent quark number, $n_{\rm cq}$, and plotted against $p_\perp/n_{\rm cq}$ and $E_\perp/n_{\rm cq}$. The re-scaled distributions coincide. The initial conditions of the expansion leading to the shown distributions are $n_{B0} = 0.21$ fm^{-3} and $T_{q0} = 176$ MeV. The final baryon and meson temperatures are $T_b = 228$ MeV and $T_m = 152$ MeV and $T_b/T_m = 3/2$.

In the model we use the simplifying assumption that the masses of baryons and mesons are equal to the sum of the masses of their constituent quarks at the freeze-out temperature and density. Thus $M_b = M_{\bar{b}} = 3M_q(n_B, T)$ and $M_m = 2M_q(n_B, T)$.

At freeze-out, the thermal equilibrium between hadrons is broken. It is assumed that both mesons and baryons have a Jüttner distribution after the freeze-out, but the temperature parameters in their respective distributions will differ. The temperature parameters T_b and T_m are determined from the condition of energy conservation: the hadron energies will be the same as the energies of their constituent quarks, with the addition of 60 MeV / hadron from the background field. See [24] for details. This will result in a temperature T_b/T_m that corresponds to the mass ratio $M_b/M_m = 3/2$.

The distribution of baryons and mesons at the point of hadronization is plotted in figure 3.8. The initial state used to generate this plot is $n_{B0} = 0.21$ fm^{-3} and $T_{q0} = 176$ MeV. In the process of recombination, the hadron temperatures increase, yielding $T_b = 228$ MeV and $T_m = 152$ MeV. The final quark mass before recombination is $M_q = 308$ MeV.

Calculation of v_2 for a source of N cells

The v_2 elliptic flow parameter can be calculated from the final hadron distributions for each hadron species. To model the asymmetry of the flow, let us divide the system into a N cells, each of which is moving with velocity $\mathbf{v}_i$, and each of which has a Jüttner distribution in their respective local rest frames. This is a generalization of the simple four-source model presented in [15], where four cells are moving in the $\pm x, \pm y$ directions, and the three-source model presented in [7].

According to the definition of v_2 (equation (3.1)), for a particle distribu-

tion $f(\mathbf{x}, \mathbf{p})$,

$$v_2 = \frac{\int d^3x \int d^3p \; f(\mathbf{x}, \mathbf{p}) \cos 2\varphi}{\int d^3x \int d^3p \; f(\mathbf{x}, \mathbf{p})}, \tag{3.16}$$

where φ is the angle of $\mathbf{p}$ relative to axis x in the plane perpendicular to the beam direction.

We are interested in the elliptic flow parameters of mid-rapidity particles as a function of $p_\perp$, so from now on we assume $p_z = 0$, and use the $(p_\perp, \varphi)$ cylindrical momentum-coordinates. Each cell is assumed to be homogeneous and the volume of cell i is denoted by V_i. Then

$$v_2(p_\perp) = \frac{\sum_i V_i \int p_\perp d\varphi \; f(p_\perp, \varphi) \cos 2\varphi}{\sum_i V_i \int p_\perp p\varphi \; f(p_\perp, \varphi)}, \tag{3.17}$$

Inserting the Jüttner distribution (3.3) into this equation, and performing the integration, we obtain

$$v_2(p_\perp) = \frac{\sum_i \tilde{N}_i \; e^{-\gamma^i M_\perp^i / T_i} \; \cos 2\varphi_0^i \; I_2(\gamma^i v_i p_\perp / T_i)}{\sum_i \tilde{N}_i \; e^{-\gamma^i M_\perp^i / T_i} \; I_0(\gamma^i v_i p_\perp / T_i)}, \tag{3.18}$$

where φ_0 is the angle in the transverse plane between the x axis and the velocity vector $\mathbf{v}_i$, $\gamma^i = 1/\sqrt{1 - v_i^2}$, and

$$\tilde{N}_i = V_i \frac{n_i}{T_i K_2(M_i/T_i)}. \tag{3.19}$$

I_k is the kth order modified Bessel function of the second kind. $M_\perp = \sqrt{M^2 + p_\perp^2}$ is the transverse mass. The calculations are detailed in [24].

If each cell has the same temperature, $T_i = T$, then the terms depending only on T cancel from the numerator and denominator, and equation (3.19)

simplifies to

$$v_2(p_\perp) = \frac{\sum_i N_i \; e^{-\gamma^i M_\perp^i/T} \; \cos 2\phi_0^i \; I_2(\gamma^i v_i p_\perp/T)}{\sum_i N_i \; e^{-\gamma^i M_\perp^i/T} \; I_0(\gamma^i v_i p_\perp/T)}, \tag{3.20}$$

where $N_i = V_i n_i$ is simply the particle number of each cell.

Two special cases are considered here: the first one is the simplest case of only two cells, moving in opposite directions with the same velocity v (see figure 3.9, top), which yields

$$v_2(p_\perp) = \frac{I_2(\gamma v p_\perp/T)}{I_0(\gamma v p_\perp/T)}. \tag{3.21}$$

The second case is a source of one larger stationary cell in the middle, and two side-cells moving in opposite directions with velocity v, as shown in the bottom panel of figure 3.9. For this latter case we obtain

$$v_2(p_\perp) = \frac{2N_s e^{-\gamma M_\perp/T} I_2(\gamma v p_\perp/T)}{2N_s e^{-\gamma M_\perp/T} I_0(\gamma v p_\perp/T) + N_c e^{-M_\perp/T}}. \tag{3.22}$$

Here N_c denotes the particle number of the middle cell, while N_s denotes the particle number of the identical side-cells.

3.4 Results and conclusions

The v_2 parameter as a function of the transverse momentum $p_\perp$ and transverse energy $E_\perp$ was calculated for the final states of expansion using the simple model of elliptic flow described in the previous section. Two configurations were considered.

First, we calculated v_2 using two cells moving in opposite direction with velocity v, as shown in figure 3.9. Both cells are assumed to have the same

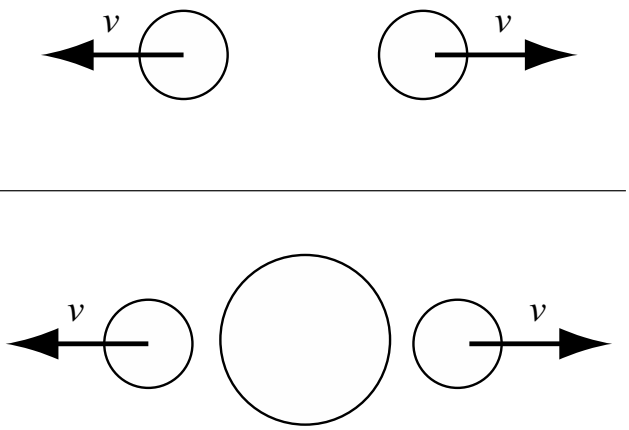

Figure 3.9: The elliptic flow can be approximated in a simple way by dividing the system into cells moving in different directions. The two simplest configurations are shown here: two cells moving in opposite directions with velocity v (top); and two moving side cells with a stationary central cell (bottom).

temperature. For this configuration v_2 is given by expression (3.21). To obtain v_2, we need the velocities of the cells. In this model, the baryons and mesons were given different flow energies per constituent quark. It was assumed that $(FE_b/n_{cq})/(FE_m/n_{cq}) = 3/2$. This assumption leads to constituent quark number scaling of $v_2(p_\perp)$ and $v_2(E_\perp)$.

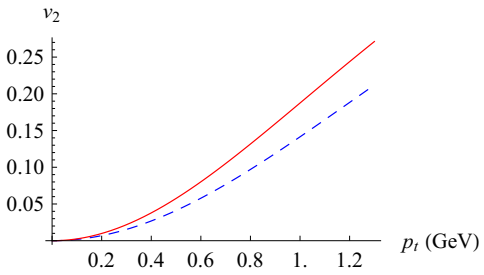

Figure 3.10: The v_2 parameter as a function of $p_\perp$, calculated with a two-cell model. The dashed blue curve represents the baryons, while the red solid curve represents the mesons. The cell velocities for baryons and mesons are $v_b = 0.26$ and $v_m = 0.21$, corresponds to a flow-energy ratio of 3/2 of the constituent quarks of the two different particle types (calculated relativistically).

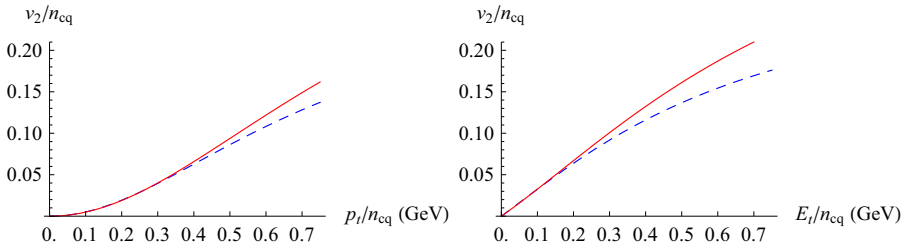

Figure 3.11: The re-scaled elliptic flow parameter, v_2/n_{cq}, as a function of $p_\perp/n_{cq}$ and $E_\perp/n_{cq}$, based on a two-cell model. The blue dashed curves represent the baryons while the solid red curves represent the mesons. The curves coincide for low $p_\perp$ value, i.e. the constituent quark number scaling is reproduced for the low $p_\perp$ region using a simple two-source model.

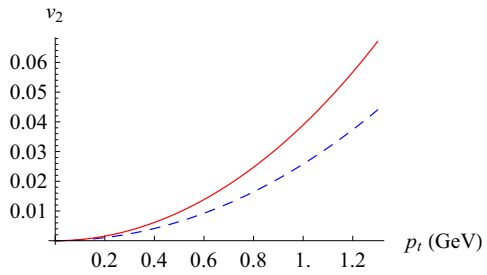

Figure 3.12: $v_2(p_\perp)$ in the three source model. The dashed blue curve represents the baryons, while the red solid curve represents the mesons. The cell velocities are the same as in the case of figure 3.10. The particle number ratio between the central and side cells is $N_c/N_s = 10$. The magnitude of v_2 is similar experimentally found values (figure 3.2).

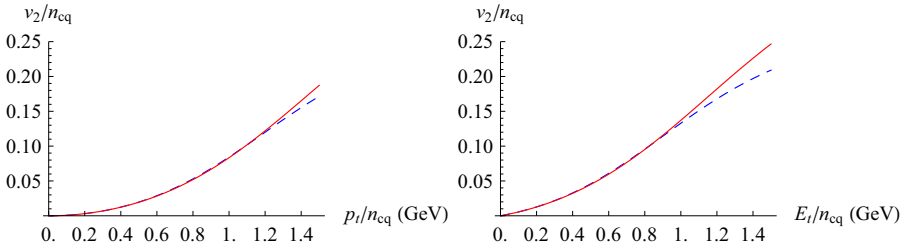

Figure 3.13: Re-scaled elliptic flow parameter calculated from the three-source model. The blue dashed curves represent the baryons while the solid red curves represent the mesons. The constituent quark number scaling is reproduced for a wider range of $p_\perp$ values than in the case of the two-cell model. Note that the bounds of the horizontal axis are wider than in figure 3.11.

The results for the same initial state that is described in the previous section are shown in figures 3.10 and 3.11. The cell velocities were taken $v_b = 0.26$ for baryons and $v_m = 0.21$ for mesons. This corresponds to a flow-energy ratio of 3/2 between the constituent quarks of baryons and mesons. As shown in figure 3.11, this assumption leads to constituent quark number scaling of v_2 in the limit of low $p_\perp$. In this simple model, there is no significant difference in the scaling behaviour between the two usual dependent variables, $p_\perp$ and $E_\perp$.

The results presented in [21] suggest that the constituent quark number scaling will be more precise if the flow asymmetry is small, and if the contribution of higher v_k ($k > 2$) Fourier coefficients is reduced. Therefore the elliptic flow parameter was also calculated for a model of one large central cell, with particle number N_c, and two smaller moving side cells with particle number N_s. The particle number ratio was set $N_c/N_s = 10$. The flow energy ratio of baryons and mesons and the side cell velocities were the same as in the case of the two-cell model. The elliptic flow parameter is given by equation (3.22) for this configuration. The v_2 curves are shown in figures 3.12 and 3.13. The magnitude of the obtained v_2 approximately matches the experimentally obtained one (compare with figure 3.2). With the three-cell model, the constituent quark number scaling is reproduced well for a wide range of $p_\perp$ values.

The simple multi-cell models considered here, with cells of equal temperatures, are just crude approximations of the realistic flow pattern, and therefore have their limitations. For example, the saturation value of v_2 for very high $p_\perp$ is always 1, therefore the constituent quark number scaling

cannot be present at high values of $p_\perp$. Nevertheless, this simple model is capable of reproducing constituent quark number scaling of the elliptic flow parameter for $p_\perp$ ranges in which it is observed in experiments.

Chapter 4

Summary

This work is a summary of three papers (references [5, 14, 24]), which deal with modelling the hadronization and freeze-out in heavy ion collisions. There is evidence that this is a non-equilibrium process, and therefore cannot be described in a quasi-statical way, assuming local phase equilibrium.

The study of dynamical phase transitions is an important subject, as it has practical applications not only in the description of nuclear collisions, but also in many other fields, e.g. in technical applications which involve high temperature detonations. Examples include gas turbines, internal combustion engines, rocket engines, etc. The correct description of some of these processes requires a relativistic approach. For example, in a rocket engine, radiation pressure has an important role in stabilizing the detonation front, therefore a relativistic description is required despite the relatively small flow velocities. Lessons learned from the study of the dynamical phase transition in heavy ion collisions can be applied to these other fields as well.

The first part of the work, based on [5, 14], analyses the final stages

of expansion in fluid dynamical models, taking into account the effects of numerical viscosity in computational approaches. A way to compute the thermodynamic parameters, such as temperature and entropy, is presented. These parameters are relevant for finding the location of the freeze-out surface.

The second part of the work, based on [24], presents a simple model of rapid and dynamical hadronization that is capable of reproducing the constituent quark number scaling of elliptic flow, as observed in experiments.

4.1 The final stages of expansion in fluid dynamical models

The Quark-Gluon Plasma was shown to behave like a low viscosity fluid in experiments, therefore fluid dynamical approaches are suitable for studying it. Except for the most trivial configurations, the equations of relativistic fluid dynamics can only be solved numerically, on a computer. However, numerical methods can only give an approximate solution to equations. The difference between the (unknown) analytic solution and the numerical solution is called the numerical error. Part of the numerical error in fluid dynamical computations arises in the form of numerical viscosity. That is, even when solving the equations of a perfect fluid, some viscosity will be present in the solution due to the effect of the finite resolution of the computational grid.

It is important to be able to estimate the effects of numerical viscosity

on the results of calculations. However, if physical viscosity is included in the fluid dynamical equations, then it is difficult to distinguish the effects of physical and numerical viscosity from each other. A possible solution to this problem is to set the numerical viscosity equal to the physical viscosity that we wish to describe. This is a viable solution when describing low viscosity fluids such as the Quark-Gluon Plasma. This approach was presented in the first part of this work.

It is important to note that the equations of perfect fluid dynamics are unstable. In real fluids, some viscosity is always present, therefore large instabilities do not always arise. Therefore it is not our goal to find the exact solution of the equations of non-viscous fluid dynamics. Instead, the numerical viscosity arising from the discretization of these equations is set equal to the (slight) physical viscosity.

The numerical fluid dynamics code that we use is based on the Particle in Cell method and is highly stable. It can run stably up to the final stages of expansion where the pressure becomes zero. Our approach is to let the fluid dynamical model run beyond the point of freeze-out. The freeze-out hypersurface can then be determined from external parameters that are not used in to solve the fluid dynamical model. The temperature and density can provide guidelines.

To be able to solve the equations of fluid dynamics, it is necessary to complement them with an equation of state that connects the pressure, baryonic density and energy density. Note, however, that quantities such as temperature and entropy do not appear in the calculation. These can be determined from the baryonic density and energy density after the code

has run. In our code, we used the simple Bag model equation of state. This equation of state yields negative pressures for low energy densities, which would indicate an (unphysical) tendency for clusterization. To avoid this, the pressure was set to zero at low energy densities. Then the entropy and temperature must be calculated in accordance with this change.

The Bag model assumes that a gas of partons is moving in a background field of constant energy density. When calculating the entropy and temperature in the energy density regions where the total pressure is zero, it is necessary to consider the exact nature of energy exchange between the parton gas and the background field. We considered three cases, each of which results in a different entropy evolution of the system.

It was found that in order for the entropy not to decrease (and to satisfy the second law of thermodynamics), it is necessary that the energy density of the background field decreases during expansion. The interaction measure was calculated as well, and compared to curves obtained from Lattice QCD calculations.

It is conjectured that the hadronization and freeze-out may proceed through a Quarkyonic phase, where the chiral symmetry is broken and the quarks gain mass. This corresponds to the gradual disappearance of the background field in these calculations.

4.2 Constituent quark number scaling in heavy ion collisions

The momentum distribution of particles created in nuclear collisions is asymmetric, primarily due to the finite impact parameter. This asymmetry is referred to as the elliptic flow. The elliptic flow is usually characterized by the second harmonic coefficient, v_2, of the momentum distribution in the plane perpendicular to the beam direction. It was observed in experiments that the v_2 parameter, when studied as a function of the transverse momentum $p_\perp$, scales according to the constituent quark number of hadrons. That is, if v_2/n_{cq} is plotted against $p_\perp/n_{\mathrm{cq}}$, the curves coincide for all hadron species. The scaling is more precise if instead of the transverse momentum, the transverse energy, $E_\perp$ is used as dependent variable.

The presence of this scaling in experimental data suggests that the elliptic flow develops in the Quark-Gluon Plasma phase, before the quarks are confined into hadrons. Thus the study of elliptic flow may provide information about the Quark-Gluon Plasma phase of matter, and the hypothetical Quarkyonic phase.

The experimentally observed constituent quark number scaling is a remarkably simple phenomenon. Therefore it is reasonable to assume that it can be reproduced by a relatively simple model. Equilibrium models are unable to reproduce the constituent quark number scaling of v_2, therefore we approached the problem using a non-equilibrium model of dynamic hadronization.

We considered a simple model of rapid and dynamic hadronization, where

the change of the effective mass of quarks was taken into account. In this model, the hadronization proceeds through the following phases: First, the chiral symmetry breaking starts and the effective quark mass increases. The chemical equilibrium between quarks and anti-quarks ceases at the same time. Then the gas of quarks and anti-quarks expands rapidly, while the effective quark mass increases. The mass was calculated as a function of temperature and density. In accordance with experimental observations, recombination into hadrons and freeze-out happens at the point when the average energy per hadron reaches 1.2 GeV / hadron. The created hadrons are not in thermal equilibrium with each other.

In this simple model it was assumed that the quark gas has Jüttner distribution. The expansion curves were computed from the condition of entropy conservation. This leads to rapid cooling of the quark gas. The quarks recombine into hadrons at the point of freeze-out, resulting in a re-heating of the matter to experimentally observed temperatures, and the production of entropy.

The v_2 parameter was calculated from the final hadron distributions using a simple multi-source model to approximate the elliptic flow. $v_2(p_\perp)$ and $v_2(E_\perp)$ was calculated assuming that the system consists of N homogeneous cells moving in different directions. Two particular cases were considered: a system made of only two cells, moving in opposite directions with the same velocity; and a stationary central cell surrounded by two smaller side cells moving in opposite directions. The first case leads to a highly asymmetric momentum distribution. The second case models a spherical momentum distribution with the addition of a small elliptic component.

The model of two cells can only reproduce constituent quark number scaling of $v_2(p_\perp)$ in the limit of small $p_\perp$ values. However, the three cell model, containing a stationary central source, yields $v_2(p_\perp)$ curves that which follow the scaling for a wide range of $p_\perp$ values.

Thus we were able to reproduce constituent quark number scaling in a simple, non-equilibrium model of hadronization.

4.3 Validity and significance of results and work of the candidate

This work is a summary of my contributions to the three articles. Our aim was to reproduce experimentally observed features, such as the constituent quark number scaling of the elliptic flow, using simple models. To reproduce every feature of a phenomenon, we need complex and detailed models. However, such models are only feasible when the phenomenon is well understood. The study of the hadronization transition in heavy ion collisions is still an open field of research. Therefore out goal was to understand the main features of this transition and the mechanisms responsible for features of the experimental data. Although the hadronization model presented here is admittedly crude, it succeeds in reproducing the constituent quark number scaling of the v_2 parameter.

My main work during the period of the doctoral research was first focused on fluid dynamical models and the final stages of the expansion of the Quark-Gluon Plasma. I described a method to correctly calculate thermodynamic

parameters during the final stages of expansion in a computational fluid dynamical model, applied the method to actual calculations, and discussed the significance of the fluid dynamical results for the hadronization transition. The second part of my work was focused on a simple non-equilibrium hadronization model. I carried out the analytic and numerical calculations related to the expansion of the quark gas and the final recombination of quarks into hadrons. I calculated and discussed the $v_2(p_\perp)$ curves obtained from the model, using simple few-source models of the elliptic flow.

List of Figures

Bibliography

[1] Piotr Bożek. Viscous evolution of the rapidity distribution of matter created in relativistic heavy-ion collisions. *Phys. Rev. C*, 77(3):034911, Mar 2008.

[2] L. Bravina, L. P. Csernai, P. Lévai, and D. Strottman. Collective global dynamics in Au+Au collisions at the BNL AGS. *Physical Review C*, 50(4):2161, 1994.

[3] J. Cleymans, H. Oeschler, K. Redlich, and S. Wheaton. Strangeness excitation functions and transition from baryonic to mesonic freeze-out. *Acta Physica Polonica B Proceedings Supplement*, 3(3):533, 2010.

[4] L. P. Csernai. *Introduction to Relativistic Heavy Ion Collisions*. John Wiley & Sons, 1994.

[5] L. P. Csernai, Y. Cheng, Sz. Horvát, V. Magas, D. Strottman, and M. Zétényi. Flow analysis with 3-dim ultra-relativistic hydro. *Journal of Physics G: Nuclear and Particle Physics*, 36(6):064032, 2009.

[6] L. P. Csernai, Y. Cheng, V. K. Magas, I. N. Mishustin, and D. Strottman. Collective flow in ultra-relativistic collisions. *Nuclear Physics A*, 834(1-4):261c–264c, 2010.

[7] L. P. Csernai and I. Mishustin. Punch-line for ncq scaling from quarkyonic matter. Unpublished.

[8] L. P. Csernai and I. N. Mishustin. Fast hadronization of supercooled Quark-Gluon plasma. *Physical Review Letters*, 74(25):5005, 1995.

[9] László P. Csernai and Joseph I. Kapusta. Dynamics of the qcd phase transition. *Physical Review Letters*, 69:737, 1992.

[10] László P. Csernai and Joseph I. Kapusta. Nucleation of relativistic first-order phase transitions. *Physical Review D*, 46:1379, 1992.

[11] László P. Csernai, Joseph I. Kapusta, and Larry D. McLerran. Strongly interacting Low-Viscosity matter created in relativistic nuclear collisions. *Physical Review Letters*, 97(15):152303–4, October 2006.

[12] C. Bernard, et al, MILC Collaboration. The equation of state for QCD with 2+1 flavors of quarks. In *Proceedings of XXIIIrd International Symposium on Lattice Field Theory*, 2005. PoSLAT2005:156,2006.

[13] Yoshimasa Hidaka, Larry D. McLerran, and Robert D. Pisarski. Baryons and the phase diagram for a large number of colors and flavors. *Nuclear Physics A*, 808(1-4):117–123, 2008.

[14] Sz. Horvát, V. K. Magas, D. D. Strottman, and L. P. Csernai. Entropy development in ideal relativistic fluid dynamics with the bag model equation of state. *Physics Letters B*, 692:277–280, 2010.

[15] P. Huovinen, P. F. Kolb, U. Heinz, P. V. Ruuskanen, and S. A. Voloshin. Radial and elliptic flow at RHIC: further predictions. *Physics Letters B*, 503(1-2):58–64, 2001.

[16] P. K. Kovtun, D. T. Son, and A. O. Starinets. Viscosity in strongly interacting quantum field theories from black hole physics. *Physical Review Letters*, 94(11):111601, 2005.

[17] Roy A. Lacey. Is there a sonic boom in the little bang at rhic? In *International Conference on Strong and Electro Weak Matter, Brookhaven National Laboratory*, 2006. arXiv:nucl-ex/0608046v1.

[18] V. K. Magas, L. P. Csernai, and D. Strottman. Effective string rope model for the initial stages of ultra-relativistic heavy ion collisions. *Nuclear Physics A*, 712(1-2):167–204, 2002.

[19] V. K. Magas, L. P. Csernai, and D. D. Strottman. Initial state of ultrarelativistic heavy ion collisions. *Physical Review C*, 64(1):014901, 2001.

[20] Larry McLerran and Robert D. Pisarski. Phases of dense quarks at large nc. *Nuclear Physics A*, 796(1-4):83–100, 2007.

[21] Denes Molnar. Parton cascade and coalescence. *Nuclear Physics A*, 774:257–266, 2006.

[22] Huichao Song and Ulrich Heinz. Multiplicity scaling in ideal and viscous hydrodynamics. *Phys. Rev. C*, 78(2):024902, Aug 2008.

[23] Aihong Tang. Summary of STAR flow results. In *INT Workshop, Seattle*, May 2010.

[24] Sven Zschocke, Szabolcs Horvát, Igor Mishustin, and László P. Csernai. Constituent quark number scaling of the elliptic flow. Manuscript, 2010.

Publications

This work describes studies in the field of statistical physics that are related to high energy heavy ion physics [1,2,3]. I have in the same period of time published other works in statistical physics which are not related to heavy ion physics, but make use of similar methods from the field of statistical physics [4,5].

Publications

1. L. P. Csernai, Y. Cheng, Sz. Horvát, V. Magas, D. Strottman, and M. Zétényi, *Flow analysis with 3-dim ultra-relativistic hydro,* **Journal of Physics G**, vol. **36**, no. 6, p. 064032, 2009.

2. Sz. Horvát, V. Magas, D. Strottman, and L. Csernai, *Entropy development in ideal relativistic fluid dynamics with the Bag Model equation of state,* **Physics Letters B**, vol. **692**, no. 4, pp. 277-280, 2010.

3. S. Zschocke, Sz. Horvát, I. Mishustin, L. P. Csernai, *Constituent quark number scaling*, Manuscript

4. Sz. Horvát, A. Derzsi, Z. Néda, and A. Balog, *A spatially explicit model for tropical tree diversity patterns*, **Journal of Theoretical Biology**, vol. **265**, no. 4, pp. 517-523, 2010.

5. Sz. Horvát, E. Á. Horváth, G. Máté, E. Káptalan, Z. Néda, *Unexpected synchronization*, **Journal of Physics: Conference Series**, vol. **182**, 012026, 2009